

KINEMATICS OF IONIZED GAS AT 0.01 AU OF TW Hya*

M. GOTO¹, A. CARMONA^{2,3}, H. LINZ¹, B. STECKLUM⁴, TH. HENNING¹, G. MEEUS^{5,6}, AND T. USUDA⁷

¹ Max-Planck-Institut für Astronomie, Königstuhl 17, D-69117 Heidelberg, Germany; mgoto@mpia.de

² ISDC, Ch. d'Ecogia 16, CH-1290 Versoix, Switzerland

³ Observatoire de Genève, University of Geneva, Ch. des Maillettes 51, 1290 Versoix, Switzerland

⁴ Thüringer Landessternwarte Tautenburg, Sternwarte 5, D-07778 Tautenburg, Germany

⁵ Astrophysikalisches Institut Potsdam, An der Sternwarte 16, 14482 Potsdam, Germany

⁶ Departamento de Física Teórica, Universidad Autónoma de Madrid, Cantoblanco, 28049 Madrid, Spain

⁷ Subaru Telescope, 650 North A'ohoku Place, Hilo, HI 96720, USA

Received 2011 April 18; accepted 2012 January 2; published 2012 February 28

ABSTRACT

We report two-dimensional spectroastrometry of Br γ emission of TW Hya to study the kinematics of the ionized gas in the star–disk interface region. The spectroastrometry with the integral field spectrograph SINFONI at the Very Large Telescope is sensitive to the positional offset of the line emission down to the physical scale of the stellar diameter (~ 0.01 AU). The centroid of Br γ emission is displaced to the north with respect to the central star at the blue side of the emission line, and to the south at the red side. The major axis of the centroid motion is P.A. = -20° , which is nearly equal to the major axis of the protoplanetary disk projected on the sky, previously reported by CO submillimeter spectroscopy (P.A. = -27°). The line-of-sight motion of the Br γ emission, in which the northern side of the disk is approaching toward us, is also consistent with the direction of the disk rotation known from the CO observation. The agreement implies that the kinematics of Br γ emission is accounted for by the ionized gas in the inner edge of the disk. A simple modeling of the astrometry, however, indicates that the accretion inflow similarly well reproduces the centroid displacements of Br γ , but only if the position angles of the centroid motion and the projected disk ellipse are a chance coincidence. No clear evidence of disk wind is found.

Key words: circumstellar matter – protoplanetary disks – stars: activity – stars: formation – stars: individual (TW Hya) – stars: pre-main sequence – techniques: high angular resolution

1. INTRODUCTION

It is commonly accepted that a protoplanetary disk dissipates inside out. Although the direct trigger is still not clear, a large number of spectral energy distributions collected by the *Spitzer Space Telescope* (e.g., Currie et al. 2008; Sicilia-Aguilar et al. 2008), as well as the direct imaging of the central cavity by the submillimeter/millimeter interferometric arrays (submillimeter array (SMA): Brown et al. 2008; Plateau de Bure Interferometer: Piétu et al. 2006), give clear observational evidence that many disks dissipate at the central part first. The innermost region of a disk (< 1 AU) is, therefore, the critical site to study how the disk dissipation starts. The structure of a disk at that radius is, however, expected to be complicated (see Dullemond & Monnier 2010 for a recent review). Dust grains evaporate in close proximity to the star. Hot gas may remain inside the inner truncation of the dust disk, but in ongoing dissipation either by accretion onto the star, disk wind/jet, or by a forming planet that sweeps out the disk.

TW Hya belongs to a small group of stars in which the disk dissipation is currently in progress (Alexander 2007 for a review of transition objects). The closeness of TW Hya to the solar system (50–60 pc; Kastner et al. 1997; Hoff et al. 1998; Mamajek 2005) makes it an exceptional laboratory to look into the central few AU of a disk (we will use $d = 51$ pc from Mamajek 2005 throughout this paper). The missing inner disk of TW Hya was first recognized by Calvet et al. (2002) through the lack of near-infrared excess, which attests the absence of hot dust close to the central star. A comprehensive multiwavelength study of the

mass distribution of the disk by Gorti et al. (2011) confirmed that the inner disk (< 3.5 AU) is indeed depleted by one to two orders of magnitude from that which is extrapolated from the surface density of the disk immediately outside. Interferometric observations also lend support to the clearing of the inner disk, although the exact location of the inner truncation is under debate (0.4–4 AU; Eisner et al. 2006; Ratzka et al. 2007; Hughes et al. 2007).

Hydrogen recombination lines are widely used to study the hot plasma near the central star, in particular in the accretion columns channeled by the magnetic fields (Uchida & Shibata 1984; Camenzind 1990; Königl 1991). However, the quantitative modeling of the line emission is still a challenge (Romanova et al. 2004; Gregory et al. 2006; Kurosawa et al. 2006, 2008), and the origin of the emission line is not completely understood, either (e.g., Kraus et al. 2008). The goal of this paper is to study the dynamics of the ionized gas inside the inner hole of a transition disk with a high angular precision afforded by two-dimensional (2D) spectroastrometry (e.g., Garcia et al. 1999; Davies et al. 2010). Spectroastrometry with a long slit spectrograph has been used for some time to study the kinematics of the emission lines of pre-main-sequence stars on the order of 1 AU (e.g., Solf & Böhm 1993; Bailey 1998). We will employ an integral field spectrograph assisted by an adaptive optics system to achieve the astrometry of the physical scale of a stellar diameter in order to deal with the ionized gas in the star–disk interface region.

2. OBSERVATION

The observations were performed by the integral field spectrograph SINFONI (Eisenhauer et al. 2003) at the Very Large

* Based on data collected by SINFONI observations [79.C-0559(B)] at the VLT on Cerro Paranal (Chile), which is operated by the European Southern Observatory (ESO).

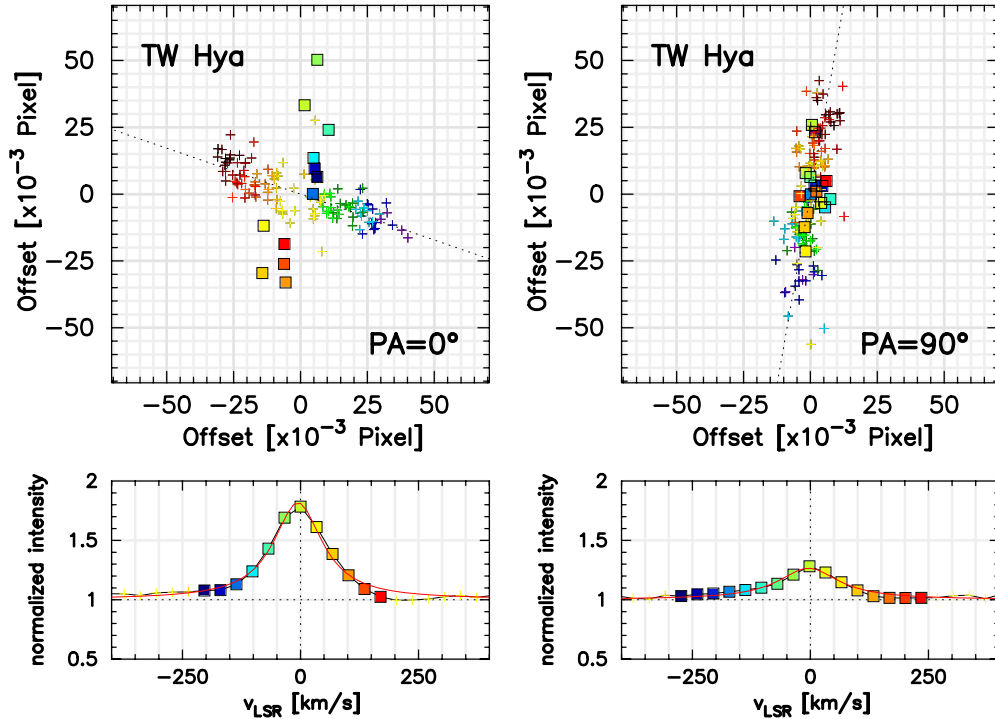


Figure 1. Top: the centroids of the PSF at the wavelengths near Br γ emission. North is up, and east is to the left. The centroids recorded with the detector column aligned to P.A. = 0° are shown in the left panel, and to P.A. = 90° in the right panel. The PSF centroids in the Br γ emission are shown with squares, and those of the continuum wavelengths are shown with crosses. Both symbols are color-coded from blue to red with the wavelength. The drifts of the PSF at the continuum wavelengths are fitted by linear functions of the wavelength, and are shown in dotted lines. Bottom: line profiles of the Br γ emission. The crosses and the squares are from the observations, color-coded in the same way as the panels above. The red lines are Lorentzian functions that best fit the observed data points.

Telescope (VLT) with the adaptive optics system MACAO (Bonnet et al. 2004). An image on the focal plane (field of view 0''.8 × 0''.8) was sliced into 32 reflective slitlets, each providing a medium resolution spectrum in the K band ($R = 4000$). The pixel scale is 12.5 mas on the detector, although the spatial sampling perpendicular to the length of the slitlets is limited by the resolution of the image slicer (25 mas). The observations were carried out with two instrumental angles, one with the detector column pointing to the north (P.A. = 0°; performed on UT 2006 January 19), and the other to the east (P.A. = 90°; on UT 2006 January 28).

3. DATA REDUCTION

3.1. Spectroscopy

The SINFONI data-reduction pipeline provides data cubes in which the monochromatic images are stacked along the wavelength. One-dimensional (1D) spectra were extracted from the data cubes by integrating the flux inside the aperture of 0''.2. The spectroscopic standard star HD 37702 (B8 V) was used to remove the telluric lines. The photospheric absorption line of HD 37702 at Br γ was removed before dividing the object spectra by subtracting a Lorentzian function fitting the absorption line profile. The wavelength calibration was performed by cross-correlating the object spectra with the atmospheric transmission curve calculated by ATRAN (Lord 1992). The error of the wavelength calibration was evaluated against the photospheric absorption lines at 2.10–2.21 μ m (Al I, Mg I, Na I), and found to be accurate to 20 km s⁻¹. The observed line velocity was converted to the velocity with respect to the

local standard of rest, using *rv* package on IRAF.⁸ The equivalent width of the line emission was reduced to $\sim 30\%$ of that on 2006 January 19 (P.A. = 0°), when we observed the object again on 2006 January 28 with the instrumental position angle 90°. The variability of Br γ emission of a similar amplitude has been reported by Eisner et al. (2011) for TW Hya.

3.2. Drift Correction

The point-spread function (PSF) of the star near Br γ emission was fit with a 2D Gaussian function at each wavelength to measure the PSF centroid. The positions of the PSF centroid have shown an overall drift along P.A. = 71° with the wavelength in the case of the instrumental angle aligned to 0° (crosses in Figure 1, left). This is apparently an instrumental effect, left uncorrected by the image alignment process in the pipeline, as the drift orientation changes by about the same amount when the instrument is rotated by 90° (the drift P.A. = -10°, Figure 1, right). The overall motion of the PSF drift was fit by a linear function of the wavelength and subtracted from the measurements. The centroid position at Br γ emission after the correction is shown in Figure 2. The motion of the emission centroid of Br γ was unfortunately aligned to the orientation of the PSF drift in the data with the instrumental angle set to P.A. = 90°. Although the results of the two observations performed with different rotation angles are qualitatively consistent, we will use the data from P.A. = 0° mostly in the following discussion, as they are less affected by the correction of the PSF drift. The locus of the centroid motion is an elongated ellipse with the

⁸ IRAF is distributed by the National Optical Astronomy Observatory, which is operated by the Association of Universities for Research in Astronomy, Inc., under cooperative agreement with the National Science Foundation.

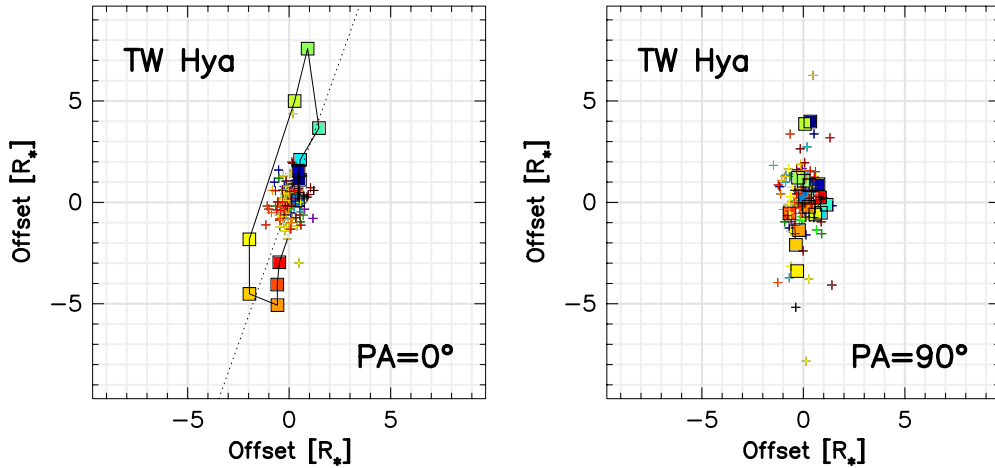


Figure 2. Same as in Figure 1, but after the correction for the PSF drift. The offsets of the PSF centroids are converted to the physical scale, assuming the distance to TW Hya is 51 pc (Mamajek 2005). The major axis of the locus is oriented to P.A. = -20° (left).

major axis aligned to P.A. = -20° in the data obtained with P.A. = 0° . The total extent of the loop is about 0.05 pixel, or 0.04 AU ($8R_*$) from the central star at the distance of TW Hya ($R_* = 0.96 R_\odot$; Yang et al. 2005).

3.3. Astrometric Accuracy

The smallest centroid offset that we can detect in the observation was estimated from the dispersion of the measured centroid positions at the continuum wavelengths. The standard deviation of the amplitudes of the centroid positions at the continuum (Figure 2) is 5×10^{-3} pixel, which is 0.003 AU at the distance of TW Hya, or less than one stellar radius. We will check below if the high astrometric accuracy achieved is consistent with the simple photon statistics. In the case that the error distribution is canonical, the accuracy of the astrometry improves from the size of PSF proportionally to the square root of the total photons detected (e.g., Bailey 1998). The size of the PSF during the observation of TW Hya measured in the median frame of the image stack was 65 mas in the full width at half maximum (FWHM). The integrated flux of the star in a raw frame was $\sim 1 \times 10^5$ ADU for 30 s of exposure time at the continuum wavelengths near Br γ emission. The total exposure time was 360 s for the object for one instrumental rotation. The photon count of the fully processed image we used for the astrometry is therefore $\sim 2.9 \times 10^6$ per spectral unit, after converting ADU to photons by the detector gain 2.4 ADU/electron. The nominal statistical error of the astrometry is therefore 0.038 mas or 3.1×10^{-3} pixel. The astrometric accuracy achieved is about 1×10^{-2} pixel in terms of the FWHM, therefore consistent with the photon statistics, though it is a few times worse than the ideal case.

We can calculate a formal error of the center of gravity for more general cases, using the realistic instrument parameters of SINFONI. The flux-weighted centroid of an emission source is given by

$$z(\lambda) = \frac{\sum_i x_i y_i}{\sum_i y_i},$$

where x_i is the 1D coordinate of the detector either row or column, and y_i is the photon count of the pixel x_i . The formal error of the centroid position σ_z is given by the pixel counts and

their errors σ_{y_i} ,

$$\sigma_z^2 = \sum_i \left[\frac{x_i \sum_i y_i - \sum_i x_i y_i}{(\sum_i y_i)^2} \cdot \sigma_{y_i} \right]^2.$$

We calculated σ_{y_i} as a squared sum of the readout noise and the shot noise of the pixel,

$$\sigma_{y_i}^2 = (\sigma_r^2 + y_i) \cdot n_{fr},$$

where n_{fr} is the number of frames averaged. The readout noise σ_r is about 10 electron for a single readout for SINFONI. The pixel count y_i is evaluated with actual observed data in the unit of electrons, and before the subtraction of the sky emission; although the sky background is negligible at the wavelength concerned (~ 0 –10 ADU). The formal error σ_z is a function of the size of the area in which the summation is calculated and is smallest when the minimum number of pixels is involved. σ_z is on the order of 0.01 pixel from 4×4 to 16×16 pixel windows, which is in reasonable agreement with 0.005 pixel that is actually achieved. The center of gravity measured in an 8×8 pixel window is compared with the measurements of the centroid by 2D Gaussian fitting and found to be consistent (Figure 3).

3.4. Test Against Artifact

A detection of a spectroastrometric signal is often tested with photospheric emission lines, in which little or no offset of the emission centroid is expected. Unfortunately, we cannot afford such a test, because Br γ emission is the only significant emission line in our spectral coverage. Instead, we measured the astrometry of PSF standard stars at the wavelength of the Br γ line with the same method that we used for TW Hya in order to show that the offset of the centroid detected is not an artifact of the measuring scheme. The PSF standard stars StKM 1-440 and CE 284 were observed on UT 2006 January 24 and 28, respectively. They are fainter than TW Hya ($K = 7.297$ mag; StKM 1-440 $K = 8.98$ mag; CE 284 $K = 9.39$ mag) and were observed with less telescope time. The astrometric accuracy achieved was therefore a few times worse, as the photon statistics are not as good as TW Hya. Nevertheless, the astrometric accuracy is good enough to negate the possible offset of the centroid at the

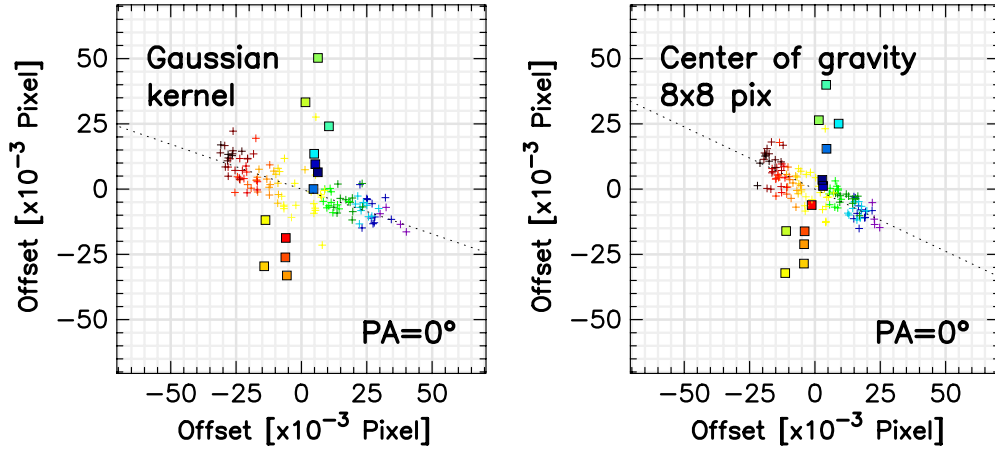


Figure 3. Comparison of the astrometry measured by Gaussian fitting (left) to that by the center of gravity (right). The center of gravity (flux-weighted center of the emission) is calculated within 8×8 pixel windows centered at the peak of the PSF. Two measurements are consistent, attesting that the positive astrometric signal at Br γ emission is not an artifact of the measuring scheme.

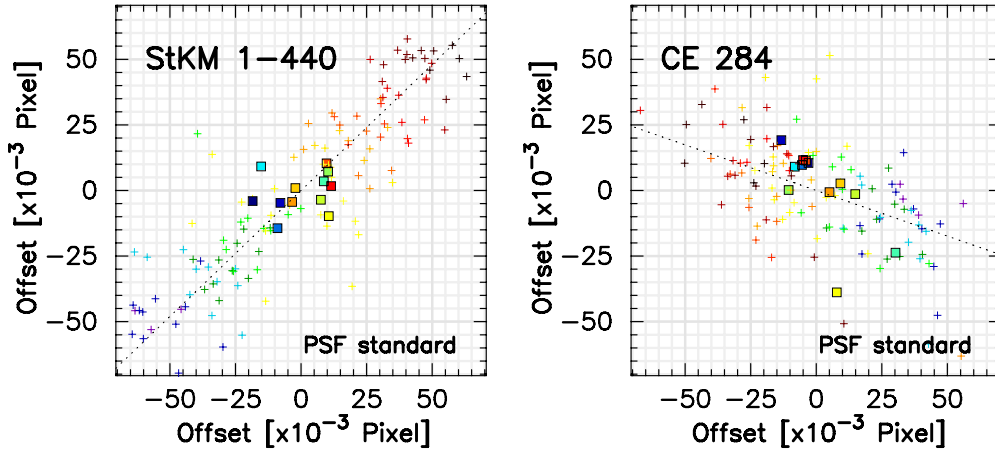


Figure 4. Spectroastrometry of two PSF standard stars StKM 1-440 and CE 284 at the wavelength of Br γ emission. Note that the astrometric accuracy of the PSF stars is not as good as TW Hya, because the photon statistic is worse. Nevertheless, it is reasonably clear that no positive astrometric signal is detected in either of the PSF standard stars, if the amplitude of the possible false signal is as large as TW Hya.

wavelength of Br γ , in the sense that it should have been detected if the astrometric signal in TW Hya were an artifact and were present in the data of StKM 1-440 and CE 284 with the same amplitudes (Figure 4).

The advantage of 2D spectroastrometry is not only a better spatial coverage and better photon statistics, but also the robustness against artifacts. Most of the artifacts that spectroastrometry suffers from, come from the use of a slit and vignetting of the source, combined with uneven illumination of a slit and a distorted PSF (Brannigan et al. 2006). In 2D spectroastrometry, we do not use a slit but slitlets, where the problem of vignetting is expected to be much smaller.

3.5. Convolution with Continuum Emission

Note that the displacement of the centroid of Br γ emission we measured above is a lower limit of the real offset of the emission line, because the PSF of the line emission is convolved with that of the continuum emission. The convolution shifts the line emission centroid toward the continuum emission source, if it is measured by fitting a Gaussian function. If we assume that the amount of the shift is proportional to the flux ratio, the convolution moves the observed

centroid to

$$r_{\text{obs}} = \frac{r_{\text{cont}} F_{\text{cont}} + r_{\text{line}} F_{\text{line}}}{F_{\text{cont}} + F_{\text{line}}},$$

where r_{line} is the intrinsic location of the centroid of the Br γ emission before the convolution, and F_{cont} and F_{line} are the flux of the continuum and the continuum-subtracted line emission, respectively. The effect of such convolution can be seen in Figure 1, where the amplitude of the centroid motion is smaller in the data with the instrumental angle set to P.A. = 90° than that to P.A. = 0° . This is reasonable, since the line intensity with respect to the continuum emission is three times smaller in P.A. = 90° . As we are only interested in the location of the line centroid relative to that of the continuum emission which is supposed to be the position of the star, we can set $r_{\text{cont}} = 0$ and r_{line} is given by

$$r_{\text{line}} = r_{\text{obs}}(1 + F_{\text{cont}}/F_{\text{line}}).$$

Such a simple correction, though frequently used, is problematic, because the correction factor $1 + F_{\text{cont}}/F_{\text{line}}$ is large at the line wings where the line emission is weak compared to the continuum emission ($F_{\text{line}}/F_{\text{cont}} \approx 0$); and the astrometric signal, as well as its error, diverge to infinity at the continuum

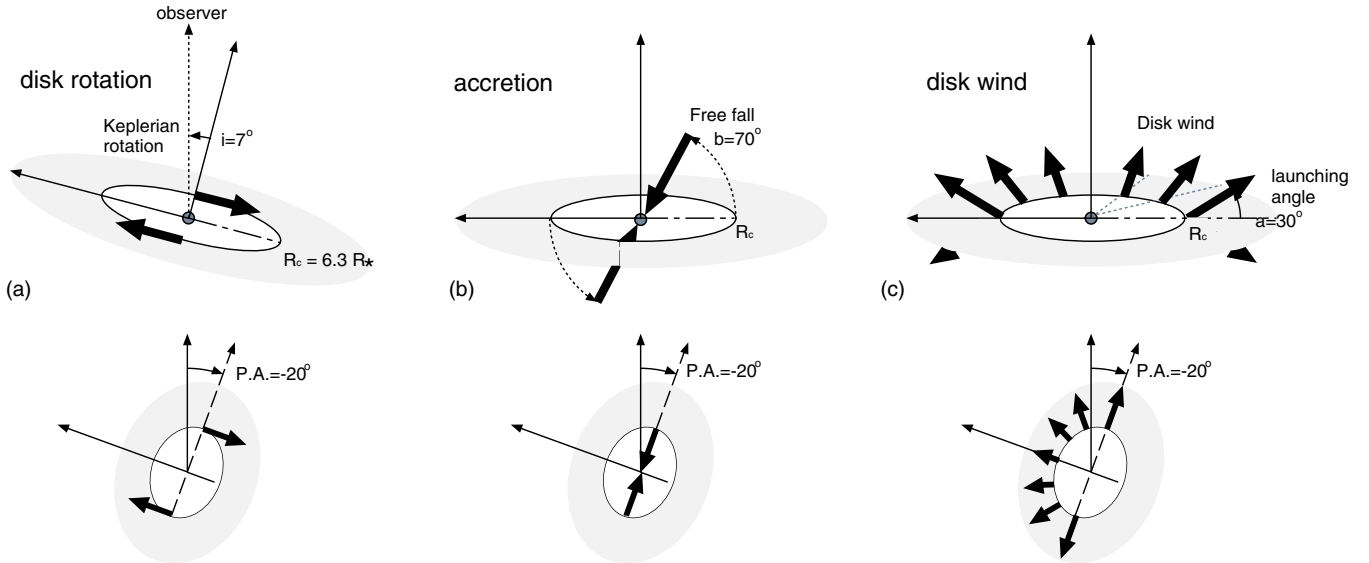


Figure 5. Schematics of the geometry assumed in the calculations of the model astrometry shown in Figure 6. The figures on the bottom are the model disks on the top row, but in projection on the sky with the proper position angle of the disk plane.

wavelengths.⁹ To avoid that, one could apply the correction only at the wavelengths where the line emission is detected above a certain significance ($F_{\text{line}}/F_{\text{cont}} \gg 0$). However, such a selective correction has the pitfall of distorting the geometry of astrometry by exaggerating astrometric signals at the border of the wavelength interval where the corrections were applied.

For these reasons, we choose not to apply the correction for the continuum convolution with the understanding that we will refrain from quantitative discussion concerning the physical scale and the complex aspects of the geometry of the ionized gas. We instead focus on the position angle of the displacement, which is more critical for the interpretation of the astrometric signal and is less affected by the convolution with the continuum emission.

4. DISCUSSION

4.1. Rotating Disk

We use three simple geometric models of the ionized gas to compare to the observed centroid motion of Br γ emission: the gas at the inner rim of a rotating disk, in an accretion flow, and in a disk wind.

In the rotating disk model, the plasma is at the inner edge of a thin disk (Figure 5(a)). The gas is assumed to be in pure Keplerian rotation with the apparent radial velocity given by $v_{\theta} = \sqrt{GM_*/R_c} \cos \theta \sin(-i)$, where i and θ are the inclination and the azimuthal angle on the disk plane, respectively. The geometry of the disk around TW Hya is reasonably well known. The disk is almost face-on ($i < 4^\circ$), according to the imaging in the scattered light by *Hubble Space Telescope*/WFPC2 and NICMOS (Krist et al. 2000; Weinberger et al. 2002). Pontoppidan et al. (2008) performed 1D spectroastrometry on the CO fundamental line and proposed a similarly small inclination angle ($i = 4^\circ \pm 1^\circ$). We use $i = 7^\circ$ reported in the submillimeter CO observation by the SMA (Qi et al. 2004, 2006) in the following models, which is constrained in a

⁹ In our case, the line-to-continuum ratio at the line center is 0.75 (P.A. = 0°) and 0.25 (P.A. = 90°), therefore the correction factor is at minimum $1 + F_{\text{cont}}/F_{\text{line}} > 2.3$ and >5 . The correction factor at the line wings is much larger than at the line center.

Table 1
Geometrical Parameters of TW Hya Stellar–Disk System Assumed Throughout the Paper

	Parameter Value	Reference
Stellar mass	$0.8 M_\odot$	Calvet et al. (2002)
Stellar radius	$0.96 R_\odot$	Yang et al. (2005)
Corotational radius	$6.3 R_*$	Johns-Krull & Valenti (2001)
Disk P.A. ^a	-20°	Present observation
Disk inclination angle	7°	Qi et al. (2004, 2006)
Distance	51 pc	Mamajek (2005)

Note. ^a The position angle of the disk plane projected on the sky.

spatially and spectroscopically resolved manner. The position angle of the disk major axis is set to P.A. = -20° , equal to the position angle of the loop observed in the present study. The stellar radius ($R_* = 0.96 R_\odot$) and the mass of the star ($M_* = 0.8 M_\odot$) are taken from Yang et al. (2005) and Calvet et al. (2002), respectively. The disk is assumed to be truncated inward at the corotation radius $R_c = 6.3 R_*$ (Johns-Krull & Valenti 2001). The stellar and disk parameters used in the models are summarized in Table 1.

The centroid of Br γ emission in this model is displaced to the north at the blueshifted wing, and moves across the disk with the wavelength along the position angle perpendicular to the disk rotation axis. This is qualitatively consistent with the observation (Figure 6(a)). However, the apparent radial velocity of the gas is too slow to match the observation. Keplerian velocity at the corotation radius is $v \sin i < 19 \text{ km s}^{-1}$. After convolution with the thermal broadening ($v = 9 \text{ km s}^{-1}$ for 10^4 K) and the instrumental resolution ($v = 75 \text{ km s}^{-1}$), the line width of Br γ emission is still too narrow by itself to explain the observed line width of 150 km s^{-1} in FWHM (Figure 6(a)).

4.2. Accretion Inflow

In the second model, the ionized gas is in a pair of accretion columns starting on a sphere at the distance of the corotation radius. The gas freefalls onto the star in straight lines symmetrically placed about the central star (Figure 5(b)). The radial velocity component of the freefalling gas is $v_r =$

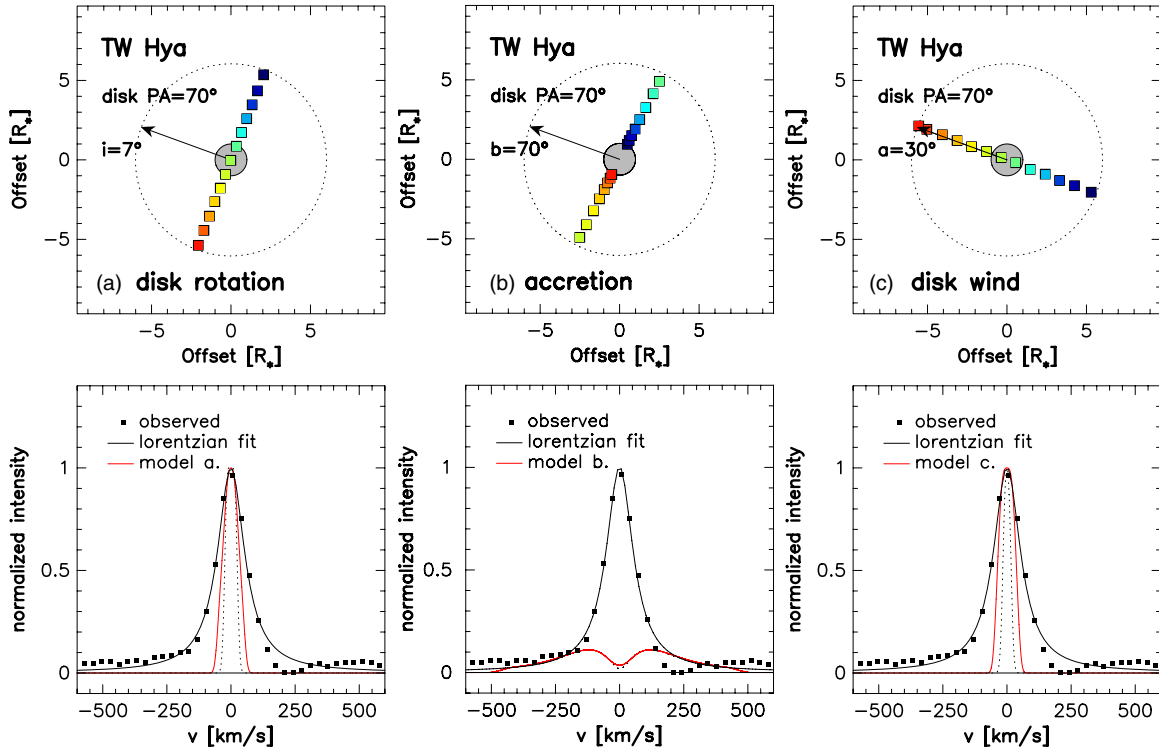


Figure 6. Models of two-dimensional astrometry for disk rotation (left), accretion flow (middle), and disk winds (right). The upper panels show the expected centroid motion of Br γ emission. The corotational radius $R_c = 6.3 R_*$ (Johns-Krull & Valenti 2001), where the disk rotation, accretion flow, or disk winds set off, is shown by a dotted line. The filled circles at the center represent the actual size of the star ($R_* = 0.96 R_\odot$; Yang et al. 2005). The lower panels show the observed line profile in dots, a Lorentzian fit to the observation as a black line, and the line profiles that come out of the models in red. The assumed geometries of the ionized gas are illustrated in Figure 5.

$\sqrt{2GM_*(1/r - 1/R_*)} \cos(i + b)$ at the distance of r with the impact angle b from the disk plane. The misalignment between the accretion columns and the disk rotation axis is assumed to be small, with $b = 70^\circ$, so that the maximum radial velocity matches the broad wings of Br γ emission ($\pm 200 \text{ km s}^{-1}$). The azimuthal angle of the inflow projected on the disk is set to -20° , so that the apparent position angle of the astrometry is consistent with the observations.

Br γ emission appears most blueshifted at the central star, as the gas in freefall is accelerated until it hits the stellar surface. The centroid of the line emission moves outward with the wavelength along the accretion column up to the corotational radius. The line emission then jumps to the other end of the corotational circle to the near-side accretion column at the red half of the emission line (Figure 6(b)). The apparent motion of the line centroid is qualitatively consistent with the observation. However, it remains unexplained how the position angle of the accretion inflow coincides with that of the disk major axis at the time of the observation. The disk of TW Hya is almost pole-on. If the accretion columns are a single pair of stream lines tied to the stellar surface by the magnetic field, the position angle projected on the sky can be of any direction at a given moment, as it rotates with the stellar rotation.

4.3. Disk Wind

In the third model, the disk wind launches outward at the corotation radius with the launching angle $a = 30^\circ$ (Figure 5(c)). The launching velocity is arbitrarily set to $v_0 = 100 \text{ km s}^{-1}$. The radial component of the disk wind at the disk azimuthal angle θ is $v_\theta = -v_0 \sin a \cos i - v_0 \cos a \sin i \sin \theta$ at the near-side of the disk.

The centroid of Br γ emission at the bluest wing appears at the intersection of the corotational circle and the disk rotation axis projected on the sky (Figure 6(c)). The centroid of the line emission moves along the disk rotational axis with the wavelength from one end to the other end of the corotation circle. The orientation of the motion is perpendicular to what is observed. Disk winds should only have a limited contribution to Br γ kinematics on the physical scale we discuss here.

5. CONCLUDING REMARK

We conclude that the observed astrometry of the Br γ emission can be accounted for either by disk rotation or accretion inflow. The disk rotation, however, does not explain the line width of Br γ emission by itself (150 km s^{-1} in FWHM), and the accretion inflow requires the arbitrary assumption that the position angle of the accretion columns is aligned to the major axis of the disk ellipse at the time of the observation. No clear evidence for disk winds is found.

It is of interest to monitor TW Hya with the spectroastrometric technique over its full rotational period. TW Hya is seen almost face-on. In the case that the alignment of the accretion columns to the position angle of the major axis of the disk is a sheer coincidence, we should see the locus of the astrometry rotating on the sky with the stellar rotation. TW Hya is the first young star–disk system where a planetary mass companion might have been found (Setiawan et al. 2008), although its presence is questioned by the recent radial velocity measurements in the infrared (Huélamo et al. 2008; Figueira et al. 2010). The rotation period of TW Hya, inferred by the photometry and the line emission variability, differs in the literature, ranging from 1.3 to 4.4 days (Siwak et al. 2011; Mekkaden 1998; Dupree et al.

2007; Batalha et al. 2002). The ill-determined rotational period critically hinders clear isolation of the radial velocity signal of the companion from the stellar activity. In the case that Br γ emission traces the accretion columns that are directly connected to the star, monitoring observation with 2D spectroastrometry will help to visualize the stellar rotation and to provide an unambiguous rotational period. The present observations were performed on the two separate nights, on 2006 January 19 (MJD 53754.20) and 2006 January 28 (MJD 53763.27). The interval was unfortunately too close to the multiples of the periods reported to date, and gives little clue to the stellar rotation.

We appreciate the constructive criticisms of the anonymous referees that substantially improved the manuscript. We thank all the staff and crew of the VLT for their valuable assistance in obtaining the data. M.G. thanks Sebastian Egner who pointed out that the calculation of astrometric accuracy is same as that of wavefront error in a Shack-Hartmann sensor. M.G. was supported by a Japan Society for the Promotion of Science fellowship.

REFERENCES

- Alexander, R. 2007, *New Astron. Rev.*, **52**, 60
- Bailey, J. A. 1998, *Proc. SPIE*, **3355**, 932
- Batalha, C., Batalha, N. M., Alencar, S. H. P., Lopes, D. F., & Duarte, E. S. 2002, *ApJ*, **580**, 343
- Bonnet, H., Abuter, R., Baker, A., et al. 2004, *The ESO Messenger*, **117**, 17
- Brannigan, E., Takami, M., Chrysostomou, A., & Bailey, J. 2006, *MNRAS*, **367**, 315
- Brown, J. M., Blake, G. A., Qi, C., Dullemond, C. P., & Wilner, D. J. 2008, *ApJ*, **675**, L109
- Calvet, N., D'Alessio, P., Hartmann, L., et al. 2002, *ApJ*, **568**, 1008
- Camenzind, M. 1990, *Rev. Mod. Astron.*, **3**, 234
- Currie, T., Kenyon, S. J., Balog, Z., et al. 2008, *ApJ*, **672**, 558
- Davies, B., Lumsden, S. L., Hoare, M. G., Oudmaijer, R. D., & de Wit, W. 2010, *MNRAS*, **402**, 1504
- Dullemond, C. P., & Monnier, J. D. 2010, *ARA&A*, **48**, 205
- Dupree, A. K., Avrett, E. H., Brickhouse, N. S., Cranmer, S. R., & Szalai, T. 2007, *arXiv:astro-ph/0702395*
- Eisenhauer, F., Abuter, R., Bickert, K., et al. 2003, *Proc. SPIE*, **4841**, 1548
- Eisner, J. A., Chiang, E. I., & Hillenbrand, L. A. 2006, *ApJ*, **637**, L133
- Eisner, J. A., Doppmann, G. W., Najita, J. R., et al. 2011, *ApJ*, **722**, L28
- Figueira, P., Pepe, F., Santos, N. C., et al. 2010, in *EAS Pub. Ser.* 42, *Extrasolar Planets in Multi-Body Systems: Theory and Observations*, ed. K. Goździewski, A. Niedzielski, & J. Schneider (Cambridge, UK: Cambridge Univ. Press), 125
- García, P. J. V., Thiébaud, E., & Bacon, R. 1999, *A&A*, **346**, 892
- Gorti, U., Hollenbach, D., Najita, J., & Pascucci, I. 2011, *ApJ*, **735**, 90
- Gregory, S. G., Jardine, M., Simpson, I., & Donati, J.-F. 2006, *MNRAS*, **371**, 999
- Hoff, W., Henning, Th., & Pfau, W. 1998, *A&A*, **336**, 242
- Huélamo, N., Figueira, P., Bonfils, X., et al. 2008, *A&A*, **489**, L9
- Hughes, A. M., Wilner, D. J., Calvet, N., et al. 2007, *ApJ*, **664**, 536
- Johns-Krull, C. M., & Valenti, J. A. 2001, *ApJ*, **561**, 1060
- Kastner, J. H., Zuckerman, B., Weintraub, D. A., & Forveille, T. 1997, *Science*, **277**, 67
- Königl, A. 1991, *ApJ*, **370**, L39
- Kraus, S., Hofmann, K., Benisty, M., et al. 2008, *A&A*, **489**, 1157
- Krist, J. E., Stapelfeldt, K. R., Ménard, F., Padgett, D. L., & Burrows, C. J. 2000, *ApJ*, **538**, 793
- Kurosawa, R., Harries, T. J., & Symington, N. H. 2006, *MNRAS*, **370**, 580
- Kurosawa, R., Romanova, M. M., & Harries, T. J. 2008, *MNRAS*, **385**, 1931
- Lord, S. D. 1992, *A New Software Tool for Computing Earth's Atmosphere Transmissions of Near- and Far-Infrared Radiation*, NASA Technical Memoir 103957 (Moffett Field, CA: NASA Ames Research Center)
- Mamajek, E. E. 2005, *ApJ*, **634**, 1385
- Mekkaden, M. V. 1998, *A&A*, **340**, 135
- Piétu, V., Dutrey, A., Guilloteau, S., Chapillon, E., & Pety, J. 2006, *A&A*, **460**, L43
- Pontoppidan, K. M., Blake, G. A., van Dishoeck, E. F., et al. 2008, *ApJ*, **684**, 1323
- Qi, C., Ho, P. T. P., Wilner, D. J., et al. 2004, *ApJ*, **616**, L11
- Qi, C., Wilner, D. J., Calvet, N., et al. 2006, *ApJ*, **636**, L157
- Ratzka, Th., Leinert, Ch., Henning, Th., et al. 2007, *A&A*, **471**, 173
- Romanova, M. M., Ustyugova, G. V., Koldoba, A. V., & Lovelace, R. V. E. 2004, *ApJ*, **610**, 920
- Setiawan, J., Henning, Th., Launhardt, R., et al. 2008, *Nature*, **451**, 38
- Sicilia-Aguilar, A., Henning, Th., Juhász, A., et al. 2008, *ApJ*, **687**, 1145
- Siwak, M., Rucinski, S. M., Matthews, J. M., et al. 2011, *MNRAS*, **410**, 2725
- Solf, J., & Böhm, K. H. 1993, *A&A*, **410**, L31
- Uchida, Y., & Shibata, K. 1984, *PASJ*, **36**, 105
- Weinberger, A. J., Becklin, E. E., Schneider, G., et al. 2002, *ApJ*, **566**, 409
- Yang, H., Johns-Krull, C. M., & Valenti, J. A. 2005, *ApJ*, **635**, 466